BIOCHEMISTRY

 Volume 45, Number 33 August 22, 2006

Articles

Structure of the Actuator Domain from the *Archaeoglobus fulgidus* Cu^+-ATPase[†,‡]

Matthew H. Sazinsky,[§] Sorabh Agarwal,[§] José M. Argüello,*[,||] and Amy C. Rosenzweig*[,§]

Departments of Biochemistry, Molecular Biology, and Cell Biology and of Chemistry, Northwestern University, Evanston, Illinois 60208, and Department of Chemistry and Biochemistry, Worcester Polytechnic Institute, Worcester, Massachusetts 01609

Received May 19, 2006; Revised Manuscript Received June 15, 2006

ABSTRACT: Copper homeostasis is maintained in part by membrane-bound P_{1B}-type ATPases that are found in all organisms and drive the transport of this essential, yet toxic, metal ion across cellular membranes. CopA from *Archaeoglobus fulgidus* is a hyperthermophilic member of this ATPase subfamily and is homologous to the human Wilson and Menkes disease ATPases. To gain insight into Cu^+-ATPase function, the structure of the CopA actuator domain (A-domain) was determined to 1.65 Å resolution. The CopA A-domain functions to couple ATP hydrolysis in the ATP binding domain (ATPBD) with structural rearrangements of critical transmembrane segments. Its fold is quite similar to that of the sarcoplasmic reticulum Ca^{2+}-ATPase (SERCA1) A-domain, with the exception of an external loop region. On the basis of sequence and structural comparisons, specific residues that probably interact with the CopA ATPBD have been identified. Comparisons to the Wilson and Menkes disease A-domains reveal the presence of an additional loop that may be associated with regulatory functions in eukaryotic Cu^+-ATPases. Finally, several mutations in the Wilson and Menkes disease ATPases occur in the A-domain, and their likely effects on function can be inferred from the CopA A-domain structure.

Cu^+-ATPases belong to the family of P_{1B}-type ATPases, a subclass of P-type ATPases that is essential for the distribution and detoxification of transition metal ions (*1*−*4*). Found in all organisms, Cu^+-ATPases couple ATP hydrolysis with the transport of Cu^+ across membranes. Excess copper, because of its biologically useful redox potential, can generate damaging free radicals and thus must be tightly controlled. In humans, improper function of Cu^+-ATPases causes Wilson and Menkes diseases (*5*). Mutations in the *ATP7B* gene encoding the Wilson disease ATPase (WND)[1] result in the accumulation of copper in the liver and brain. As a consequence, Wilson disease patients suffer from neurologic and hepatic disorders. Conversely, mutations in the Menkes ATPase (MNK), or the *ATP7A* gene, result in poor copper uptake from the intestine. Ultimately, this copper deficiency manifests itself as neurodegeneration and connective tissue abnormalities.

P_{1B}-type ATPases, while maintaining central structural elements common to all P-type ATPases, have a distinct architecture (*1*, *3*, *6*). Most significantly, they differ from

[†] This work was supported by NIGMS Grant GM58518 (A.C.R.) and NSF Grant MCM-0235165 (J.M.A.). M.H.S. was supported by NRSA Fellowship GM073457.

[‡] PDB accession code 2HC8.

* To whom correspondence should be addressed. A.C.R.: telephone, 847-467-5301; fax, 847-467-6489; e-mail, amyr@northwestern.edu. J.M.A.: telephone, 508-831-5326; fax, 508-831-5933; e-mail, arguello@wpi.edu.

[§] Northwestern University.

[||] Worcester Polytechnic Institute.

[1] Abbreviations: A-domain, actuator domain; ATPBD, ATP binding domain; MNK, Menkes disease protein; N-domain, nucleotide binding domain; MBD, N-terminal metal binding domain; P-domain, phosphorylation domain; rmsd, root mean square deviation; SERCA1, sarcoplasmic reticulum Ca^{2+}-ATPase; WND, Wilson disease protein.

10.1021/bi0610045 CCC: $33.50
Published on Web 07/27/2006

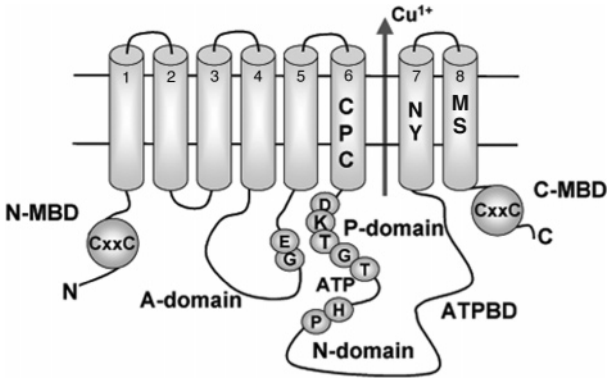

FIGURE 1: Membrane topology of the *A. fulgidus* Cu^+-ATPase.

their P_2-type and P_1-type counterparts in the arrangement and number of transmembrane helices. P_{1B}-type ATPases consist of eight transmembrane (TM) helices, several cytosolic loops, and cytosolic N- and C-terminal metal binding domains (MBD) (Figure 1) (*1*, *6*). The large cytoplasmic loop between TM6 and TM7 comprises the ATP binding domain (ATPBD), which includes the phosphorylation (P) and nucleotide binding (N) domains. The region between TM4 and TM5 bears little sequence similarity to the corresponding region in other ATPase subgroups, but because of its length and the presence of a highly conserved TGE(P/X) sequence, it is considered equivalent to the actuator or A-domain of the P_2-type ATPases. There is no structural or functional information on the role of the short loop between segments TM2 and TM3.

Heavy metal ATPases also have extended cytosolic N- and C-terminal regions that bind metals and differ significantly in sequence and length among the various P_{1B}-ATPase subgroups (*1*, *7*, *8*). For Cu^+-ATPases, the N-termini comprise one to six metal binding domains (MBDs) that are structurally similar to the cytosolic Atx1-like copper chaperones and contain conserved CXXC metal binding sequences (*2*, *6*, *7*, 9). The human WND and MNK proteins contain six N-terminal MBDs, the *Drosophila melanogaster* homologue contains four, the *Saccharomyces cerevisiae* and *Escherichia coli* homologues contain two, and the corresponding protein from the hyperthermophile *Archaeoglobus fulgidus* has only one MBD. The N-terminal MBDs are not required for ion transport but play a regulatory role by controlling enzyme turnover and the targeting of Cu^+-ATPases to various membrane compartments in eukaryotes (*10*−*14*). Cu^+-ATPases, like other P-type ATPases, have transmembrane metal binding sites that coordinate ions during transport. For Cu^+-ATPases, these sites consist of strictly conserved residues located in transmembrane fragments TM6, TM7, and TM8, of which all cluster near the ATPBD (*1*, *15*, *16*) (Figure 1). The arrangement of the transmembrane metal binding sites relative to the ATPBD is analogous to that found in the better characterized P_2-type Na,K- and Ca^{2+}-ATPases (*4*, *17*, *18*).

The Cu^+-ATPases follow the Post-Albers catalytic cycle in which metal ion translocation is coupled to phosphorylation of an aspartate residue in the conserved sequence DKTGT (*19*−*22*). The conformational changes accompanying Cu^+ translocation are not well understood due to the relative absence of detailed structural information on P_{1B}-type ATPases. Moreover, recent progress in structural characterization of the sarcoplasmic reticulum Ca^{2+}-ATPase (SERCA1), a P_2-type ATPase (*23*−*26*), cannot be readily extrapolated to P_{1B}-ATPases since the two systems differ in overall architecture. The domains present in both, such as the ATPBD and the transmembrane segments involved in ion coordination, share little sequence homology and thus cannot be modeled reliably.

To advance the understanding of P_{1B}-type ATPase function, we are using *A. fulgidus* CopA as a model system. This hyperthermophilic Cu^+-ATPase can be heterologously expressed in a fully functional form and contains all of the structural elements required for ATP-driven Cu^+ efflux (*12*, *15*, *16*, *27*). To obtain high-resolution structural information, we are characterizing independently folded cytoplasmic domains associated with ATP hydrolysis and energy transduction (the N-, P-, and A-domains). During the catalytic cycle, these domains undergo critical conformational changes directly coupled to the transmembrane helix rearrangements responsible for ion translocation. We previously determined the crystal structure of the *A. fulgidus* CopA ATPBD (*27*). Here we describe the 1.65 Å resolution structure of the cytoplasmic loop between TM4 and TM5, which is structurally, and likely functionally, similar to the A-domain in P_2-type ATPases. Based on studies of various P_2-type ATPases, this domain is expected to undergo significant positional rearrangements upon metal binding and the subsequent transition from the E1P to the E2P catalytic states (*28*). Analysis of the CopA A-domain structure allows the identification of key catalytic elements, suggests putative regions involved in regulatory interactions, and provides new insight into the structural basis of Wilson and Menkes diseases.

MATERIALS AND METHODS

Cloning and Purification of the A-Domain. The *A. fulgidus* CopA A-domain (residues 213−326) was PCR amplified from CopA cDNA contained in a pCRT7/NT-TOPO His vector (Invitrogen) by using the primers 5′-GCCCTTG-GTCTCTAATGGGGGAGGCCATAAAGAAGCTC-3′ and 5′-CGGGAAGGTCTCTGCGCTGCCCATCGCGTCCTCGA-CCAG-3′, which introduce 5′ and 3′ *Bsa*I restriction sites. The purified PCR product and the plasmid pPR-IBA1 (IBA) were digested with *Bsa*I, purified, and ligated to create the plasmid pCOPAD. The final construct contains a 10 amino acid streptactin tag (SAWSHPQFEK) fused to the C-terminus of the protein. DNA sequencing confirmed the presence and accuracy of the A-domain gene fragment in the pCOPAD vector.

BL21Star(DE3)pLysS *E. coli* cells (Invitrogen) carrying the plasmid pSJS1240 encoding for rare tRNAs ($tRNA^{arg}$-AGA/AGG and $tRNA^{ile}$AUA) (*29*) were transformed with pCOPAD and used for heterologous protein expression. Cell cultures were grown at 37 °C in 1 L of Luria−Bertani media supplemented with 20 mg/L chloramphenicol, 70 mg/L spectinomycin, and 100 mg/L carbanocillin. At an OD_{600} of ~0.7, protein expression was induced with 200−500 μM IPTG. After 3−4 h, the cells were harvested by centrifugation at 6000*g* for 5 min, frozen in liquid nitrogen, and stored at −80 °C until further use.

The cells were thawed in a buffer containing 100 mM Tris (pH 8.0), 150 mM NaCl, 5 mM $MgSO_4$, 50 units of DNase,

Table 1: Data Collection, Phasing, and Refinement Statistics

	Se SAD	native
data collection		
beamline	SER-CAT (sector 22)	DND-CAT (sector 5)
wavelength (Å)	0.979	0.979
resolution (Å)[a]	30−2.15	30−1.65
unique observations	6889	14467
total observations	46871	99462
completeness (%)	99.1 (93.8)	97.5 (85.5)
redundancy	6.8 (6.0)	6.9 (5.5)
I/σ	16.5 (13.9)	18.8 (2.4)
R_{sym}[b] (%)	5.6 (11.2)	8.3 (38.9)
Se sites used for phasing	2	
figure of merit (after density modification)	0.27 (0.51)	
refinement		
R_{work} (%)[c]		19.8
R_{free} (%)[d]		24.2
molecules in ASU		1
no. of protein non-hydrogen atoms		15307
no. of non-protein atoms		1042
rmsd bond length (Å)		0.0065
rmsd bond angle (deg)		1.28
average *B*-value (Å^2)		37.7

[a] Values in parentheses are for the highest resolution shell. [b] $R_{sym} = \sum_i\sum_{hkl}|I_i(hkl) - \langle I(hkl)\rangle|/\sum_{hkl}\langle I(hkl)\rangle$, where $I_i(hkl)$ is the ith measured diffraction intensity and $\langle I(hkl)\rangle$ is the mean of the intensity for the Miller index (hkl). [c] $R_{work} = \sum_{hkl}||F_o(hkl)| - |F_c(hkl)||/\sum_{hkl}|F_o(hkl)|$. [d] $R_{free} = R_{work}$ for a test set of reflections (5%).

and 1 mM PMSF and lysed by sonication for 10 min by using 30 s pulses with a 30 s rest between each pulse. Cell debris was removed by centrifugation at 163000*g* for 1 h, after which the supernatant was filtered through a 0.22 μm membrane and loaded onto a streptactin column (Qiagen). The protein was purified according to the manufacturer's protocol and then exchanged into a buffer containing 20 mM MOPS (pH 7.0), 20 mM NaCl, and 5% glycerol by using an Amicon ultra YM-5 spin concentrator. At a concentration of 10−30 mg/mL, the protein was flash frozen in liquid nitrogen and stored at −80 °C. The theoretical extinction coefficient of $\epsilon_{280} = 6990\ M^{-1}\ cm^{-1}$ was used to estimate the concentration of the A-domain by optical spectroscopy. Selenomethionine-labeled protein was generated by growing the cells in LeMaster's media (*30*) supplemented with 10 mg/L selenomethionine. The protein was expressed and purified as described above.

Crystallization, Data Collection, and Structure Determination. The A-domain was crystallized by using the hanging drop vapor diffusion method at room temperature by combining 2 μL of protein at 10 mg/mL with 1 μL of a precipitant solution comprising 100 mM Tris (pH 8.5), 1.8 M $(NH_4)_2SO_4$, and 7.5% glycerol and 1 μL of a microseed solution in the precipitant buffer. Thick rectangular crystals and thin needles appeared within 3−5 days. Prior to data collection, the crystals were transferred to a cryosolution containing 100 mM Tris (pH 8.5), 1.8 M $(NH_4)_2SO_4$, and 25% glycerol and flash frozen in liquid nitrogen. Data were collected at 100 K at the Advanced Photon Source (APS) beamlines 5ID and 23ID, which are operated by DND-CAT and SER-CAT, respectively.

The crystals belong to the space group *C*2 with unit cell dimensions $a = 111.3$ Å, $b = 29.4$ Å, $c = 40.0$ Å, and $\beta = 110.5°$. The data were either integrated by using HKL2000 (*31*) or MOSFLM (*32*) and scaled with SCALEPACK (*31*) or SCALA (*33*). The initial phases were determined by single wavelength anomalous dispersion (SAD) using the program SOLVE (*34*) and the Se peak data set (Table 1). A model of the A-domain was built with XtalView (*35*), and refinements were carried out with CNS (*36*) (Table 1). A Ramachandran plot calculation with PROCHECK (*37*) indicates that 97.9% of the residues occupy the favored regions with the remainder in generously allowed regions.

RESULTS AND DISCUSSION

Global Fold. The A-domain comprises ten β-strands and two α-helices at the N- and C-termini. These cytosolic helices extend toward the membrane-spanning helices that ordinarily

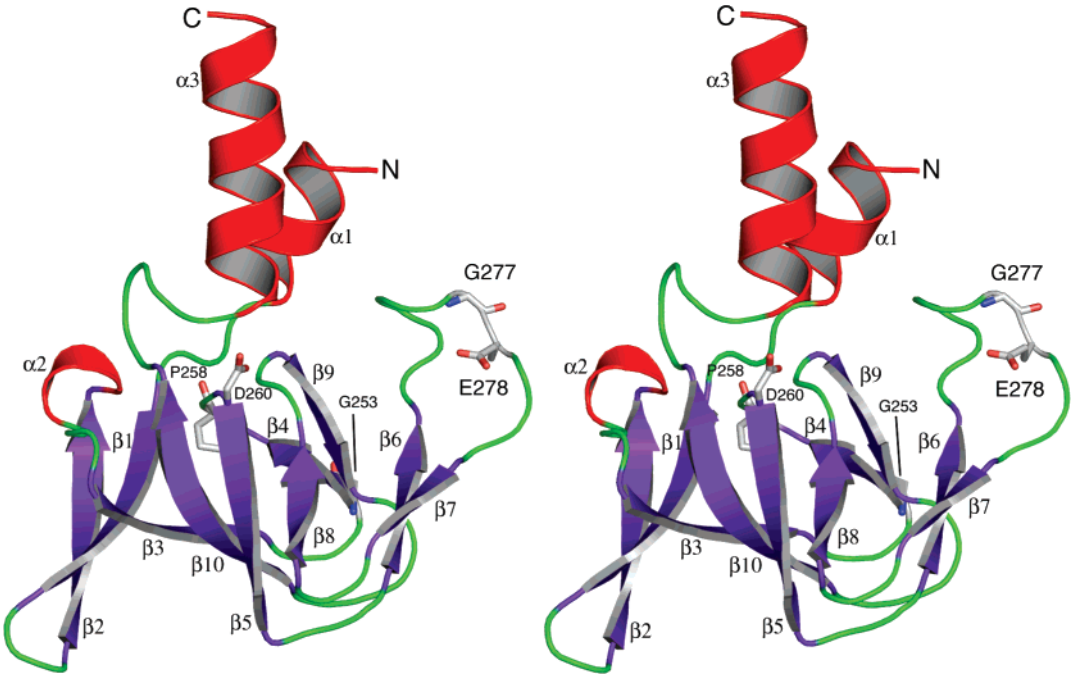

FIGURE 2: Stereoview of the CopA A-domain structure. Residues conserved among all P-type ATPases are shown as stick representations.

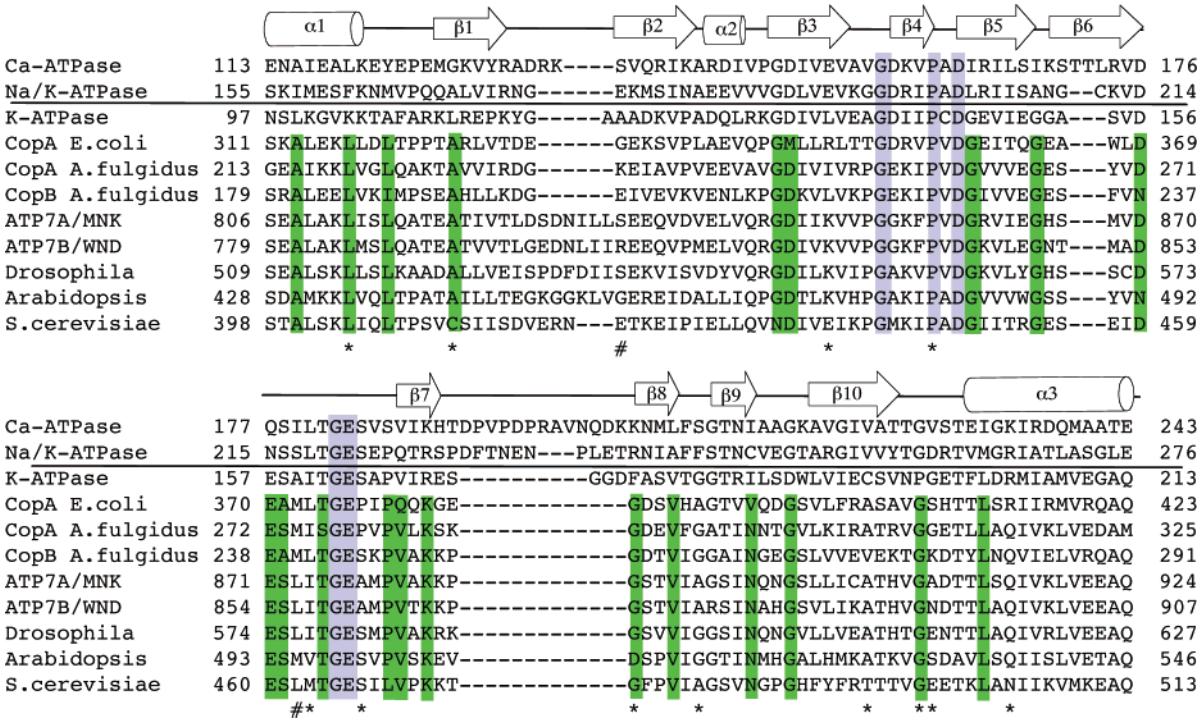

FIGURE 3: Sequence alignments of the A-domains from P_{1B}-type, P_{1A}-type, and P_2-type ATPases. Sequences above the line correspond to representative P_2-type family members. Residues highlighted in gray are highly conserved among all ATPases, and residues highlighted in green are highly conserved among Cu^+-ATPases. WND and MNK missense mutations are denoted by an asterisk (*) and pound sign (#), respectively. Sequences and accession numbers used for the alignments are as follows: Ca-ATPase, *Oryctolagus cuniculus* (2AGV_B); Na/K-ATPase, *Homo sapiens* (AAC50131); K-ATPase/KdpB, *E. coli* (NP_41522); CopA, *E. coli* (Q59385); CopA, *A. fulgidus* (O29777); CopB, *A. fulgidus* (O30085); MNK, *H. sapiens* (Q04656); WND, *H. sapiens* (P35670); ATP7, *D. melanogaster* (NP_572756); RAN1, *Arabidopsis thaliana* (Q9S7J8); CCC2, *S. cerevisiae* (P38995).

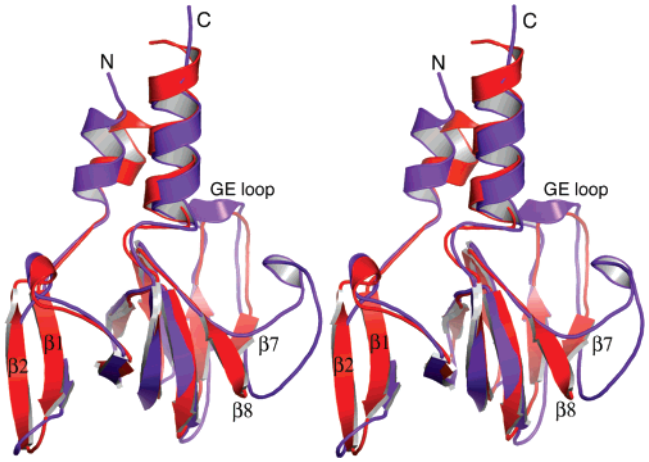

FIGURE 4: Superposition of the CopA (red) and SERCA1 (purple) A-domains in stereo.

would be found in the full-length protein (Figure 2). The highly conserved GE sequence (Figure 3) resides in the middle of a 10 amino acid solvent-accessible loop between β6 and β7 (the GE loop). The geometric configuration of the GE loop presumably facilitates interactions with the ATPBD P-domain (*38*). The other residues conserved among the different P_1- and P_2-type ATPases localize to the core of the A-domain and are probably important for proper folding.

A superimposition of the SERCA1 and CopA A-domains reveals that their folds are highly conserved and have an rms deviation of 1.1 Å between all backbone atoms even though the sequence identity is just 26% (Figure 4). The structural similarity between the CopA and SERCA1 A-domains suggests they may play similar catalytic roles in their respective full-length proteins. Notably, the CopA A-domain structure differs from representative P_2-type pumps in the absence of a 7−10 amino acid loop between β7 and β8 (Figure 3). Crystal structures of SERCA1 indicate that this loop interacts with the ATPBD N-domain in the ATP-bound E2 form of the enzyme (*24*−*26*, *39*). Its absence suggests that this interaction is not crucial for Cu^+-ATPase function.

Interactions with the ATPBD. During the catalytic cycle, the A-domain of P-type ATPases plays a central role in a complex series of domain movements and interactions that couple ATP hydrolysis with the translocation of ions across the membrane (*40*−*43*). By analogy to the SERCA1 structures, specific regions of the CopA A-domain that may interact with the CopA ATPBD can be identified. In the E1 state, the small region between β3 and β4 of the A-domain is likely to interact with the ATPBD P-domain (Figure 5A) (*24*). Upon conversion to the E2 state, the GE loop is expected to insert into the ATPBD cleft such that the conserved glutamate interacts with the phosphorylated aspartate within the conserved DKTGT loop of the P-domain (*23*, *28*, *38*, *39*). The relatively long helices at the N- and C-termini of the A-domain, of which only small portions are present in the current crystal structure, provide flexibility and sufficient distance from the transmembrane region to allow the GE and DKTGT loops to interact. In addition, these helices likely form contacts with helices from the P-domain (*38*). Consistent with these proposed interactions, the GE loop of the CopA A-domain has a relatively negative electrostatic surface potential (Figure 5B) whereas the ATPBD near the conserved DKTGT loop has a slightly

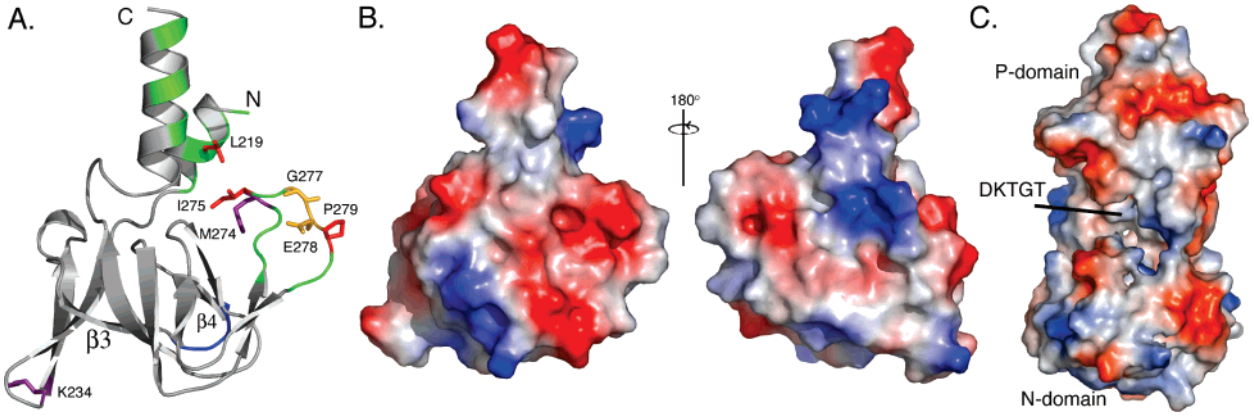

FIGURE 5: Cytosolic domain interactions. (A) Surfaces of the CopA A-domain predicted to interact with the ATPBD. Residues that interact with the E1 form of the protein are colored blue, and those that interact when the E2 form is achieved are colored green. WND mutations that may influence domain interactions are shown as red stick representations while MNK mutations are colored purple. The conserved residues of the GE loop are shown as yellow stick representations. (B) A-domain surface color-coded according to electrostatic potential: red, −10 kT; white, 0 kT; blue, +10 kT. The orientation is the same as depicted in (A). (C) Electrostatic surface potential of the CopA ATPBD. The surfaces are colored as in (B).

positive electrostatic surface potential that is complementary (Figure 5C) (*27*). As suggested by the SERCA1 structures (*28*, *38*, *39*), the predicted result of these interactions is the displacement of the A-domain and the structural rearrangement of several transmembrane helices. Because of differences in the topologies of the CopA and SERCA1 transmembrane regions, helical movements in the transmembrane region may differ for CopA.

Interactions with the MBD. The presence of regulatory domains and phosphorylation sites at the N-termini of various P_2-type ATPases suggests functional interactions between this region and the central catalytic loops (*44*−*46*). The N-terminal MBDs are unique to P_{1B}-type ATPases (*2*, *7*). Like WND (*47*), the CopA N-terminal MBD probably receives Cu^+ ions from an Atx1-like chaperone. For *A. fulgidus* CopA, metal binding to this region appears to be necessary for maximum enzyme turnover (*15*). This kinetic effect suggests that copper binding may affect specific interactions between the MBD and the other cytosolic domains. In the SERCA1 structures, a helix−turn−helix motif at the N-terminus interacts with the surface of the A-domain that is farthest away from the catalytically essential GE loop. Because of this interaction, movements in the A-domain can induce helical changes in TM1 and the subsequent opening of the lumenal ion gates (*38*). By analogy, copper binding to the CopA MBD may affect interactions with the A-domain and, in turn, rate-limiting conformational transitions.

It should also be noted that interactions between the N-terminus and the cytosolic domains may differ depending on the organism. For example, WND MBDs 1−4 interact with the ATPBD N-domain in the absence of copper, presumably through contacts with a 39 amino acid loop not found in prokaryotic Cu^+-ATPases (*48*). The addition of Cu^+ alters these interactions and results in WND relocalization from the *trans*-Golgi network to the cytoplasmic vesicles (*10*, *48*). Sequence comparisons between the A-domains of eukaryotic and prokaryotic Cu^+-ATPases indicate that the former have a small, 3−6 amino acid insert between β1 and β2 (Figure 3). This longer loop may be responsible for mediating interactions between the A-domain and the multiple MBDs in eukaryotic Cu^+-ATPases.

Structural Significance of A-Domain WND and MNK Mutations. The A-domain structure provides new insight into Wilson and Menkes disease-causing mutations (Figure 3) (*5*). Mapping these mutations onto the CopA A-domain suggests that 9 of the 12 known missense mutations in WND are located in the interior of the protein. These mutations may therefore affect the folding and stability of the domain rather than specific interactions with other cytosolic loops. This finding is consistent with the observation that pathogenic mutations altering normal protein folding and trafficking are more frequent than those affecting protein function (*49*). The other three mutations probably disrupt interactions with the ATPBD. Mutations at positions I275 and P279 (I857T and A861T in WND) likely affect the configuration of the GE loop, and the mutation at position L219 (L813Y in WND) in the N-terminal α-helix may sterically prevent interaction with the ATPBD (Figure 5A). For MNK, only two missense mutations are known to localize to the A-domain (*50*). The first is located at K234 (S833G in MNK), which is the first residue in strand β2. The second occurs at M274 (L873R in MNK) in the GE loop. The S833G mutation may disrupt the A-domain fold and could also affect domain interactions by altering the loop between β1 and β2 that is found only in eukaryotes. Like the WND mutations, the L873R MNK mutation presumably affects the configuration of the GE loop and prevents proper interactions between the actuator and ATP binding domains.

In sum, the *A. fulgidus* CopA A-domain structure offers the first glimpse of an actuator domain from a heavy metal transporting P_{1B}-type ATPase. Despite the low sequence identity, the A-domain fold is highly conserved between CopA and SERCA1, suggesting Cu^+-ATPases may utilize a similar sequence of cytoplasmic domain interactions for metal ion transport. Finally, the A-domain structure provides further insight into the molecular basis of Wilson disease and Menkes syndrome mutations.

ACKNOWLEDGMENT

We thank the staff at DND-CAT and SER-CAT for assistance with data collection.

REFERENCES

1. Argüello, J. M. (2003) Identification of ion-selectivity determinants in heavy-metal transport P1B-type ATPases, *J. Membr. Biol. 195*, 93−108.
2. Axelsen, K. B., and Palmgren, M. G. (1998) Evolution of substrate specificities in the P-type ATPase superfamily, *J. Mol. Evol. 46*, 84−101.
3. Pedersen, P. L., and Carafoli, E. (1987) Ion motive ATPases 1. Ubiquity, properties, and significance to cell function, *Trends Biochem. Sci. 12*, 146−150.
4. Møller, J. V., Juul, B., and le Maire, M. (1996) Structural organization, ion transport, and energy transduction of P-type ATPases, *Biochim. Biophys. Acta 1286*, 1−51.
5. Cox, D. W., and Moore, S. D. (2002) Copper transporting P-type ATPases and human disease, *J. Bioenerg. Biomembr. 34*, 333−338.
6. Lutsenko, S., and Kaplan, J. H. (1995) Organization of P-type ATPases: Significance of structural diversity, *Biochemistry 34*, 15607−15613.
7. Arnesano, F., Banci, L., Bertini, I., Ciofi-Baffoni, S., Molteni, E., Huffman, D. L., and O'Halloran, T. V. (2002) Metallochaperones and metal-transporting ATPases: A comparative analysis of sequences and structures, *Genome Res. 12*, 255−271.
8. Baxter, I., Tchieu, J., Sussman, M. R., Boutry, M., Palmgren, M. G., Gribskov, M., Harper, J. F., and Axelsen, K. B. (2003) Genomic comparison of P-type ATPase ion pumps in *Arabidopsis* and rice, *Plant Physiol. 132*, 618−628.
9. Rensing, C., Ghosh, M., and Rosen, B. P. (1999) Families of soft-metal-ion-transporting ATPases, *J. Bacteriol. 181*, 5891−5897.
10. Cater, M., Forbes, J., La Fontaine, S., Cox, D., and Mercer, J. F. (2004) Intracellular trafficking of the human Wilson protein: the role of the six N-terminal metal binding sites, *Biochem. J. 380*, 805−813.
11. Lutsenko, S., and Petris, M. J. (2003) Function and regulation of the mammalian copper-transporting ATPases: insights from biochemical and cell biological approaches, *J. Membr. Biol. 191*, 1−12.
12. Mandal, A. K., Yang, Y., Kertesz, T. M., and Argüello, J. M. (2004) Identification of the transmembrane metal binding site in Cu^+-transporting P_{IB}-type ATPases, *J. Biol. Chem. 279*, 54802−54807.
13. Strausak, D., La Fontaine, S., Hill, J., Firth, S. D., Lockhart, P. J., and Mercer, J. F. B. (1999) The role of GMXCXXC metal binding sites in the copper-induced redistribution of the Menkes protein, *J. Biol. Chem. 274*, 11170−11177.
14. Voskoboinik, I., Mar, J., Strausak, D., and Camakaris, J. (2001) The regulation of catalytic activity of the Menkes copper-translocating P-type ATPase, *J. Biol. Chem. 276*, 28620−28627.
15. Mandal, A. K., and Argüello, J. M. (2003) Functional roles of metal binding domains of the *Archaeoglobus fulgidus* Cu^+-ATPase CopA, *Biochemistry 42*, 11040−11047.
16. Mandal, A. K., Cheung, W. D., and Argüello, J. M. (2002) Characterization of a thermophilic P-type Ag^+/Cu^+-ATPase from the extremophile *Archaeoglobus fulgidus*, *J. Biol. Chem. 277*, 7201−7208.
17. Jorgensen, P. L., Håkansson, K. O., and Karlish, S. J. D. (2003) Structure and mechanism of Na,K-ATPase: Functional sites and their interactions, *Annu. Rev. Physiol. 65*, 817−849.
18. Peluffo, R. D., Lingrel, J. B., Argüello, J. M., and Berlin, J. R. (1997) Changes to Na,K-ATPase alpha-subunit E779 separate the structural basis for VM and ion dependence of Na,K-pump current, *Ann. N.Y. Acad. Sci. 834*, 339−342.
19. Albers, R. W. (1967) Biochemical aspects of active transport, *Annu. Rev. Biochem. 36*, 727−756.
20. Bull, P. C., and Cox, D. W. (1994) Wilson disease and Menkes disease: New handles on heavy-metal transport, *Trends Genet. 10*, 246−252.
21. Post, R. L., Hegyvary, C., and Kume, S. (1972) Activation by adenosine triphosphate in the phosphorylation kinetics of sodium and potassium ion transport adenosine triphosphatase, *J. Biol. Chem. 247*, 6530−6540.
22. Solioz, M., and Camakaris, J. (1997) Acylphosphate formation by the Menkes copper ATPase, *FEBS Lett. 412*, 165−168.
23. Sørensen, T. L., Møller, J. V., and Nissen, P. (2004) Phosphoryl transfer and calcium ion occlusion in the calcium pump, *Science 304*, 1672−1675.
24. Toyoshima, C., Nakasako, M., Nomura, H., and Ogawa, H. (2000) Crystal structure of the calcium pump of sarcoplasmic reticulum at 2.6 Å, *Nature 405*, 647−655.
25. Toyoshima, C., Nomura, H., and Tsuda, T. (2004) Lumenal gating mechanism revealed in calcium pump crystal structures with phosphate analogues, *Nature 432*, 361−368.
26. Toyoshima, C., and Nomura, H. (2002) Structural changes in the calcium pump accompanying the dissociation of calcium, *Nature 418*, 605−611.
27. Sazinsky, M. H., Mandal, A. K., Argüello, J. M., and Rosenzweig, A. C. (2006) Structure of the ATP binding domain from the *Archaeoglobus fulgidus* Cu^+-ATPase, *J. Biol. Chem. 281*, 11161−11166.
28. Toyoshima, C., and Inesi, G. (2004) Structural basis of ion pumping by Ca^{2+}-ATPase of sarcoplasmic reticulum, *Annu. Rev. Biochem. 73*, 269−292.
29. Kim, R., Sandler, S. J., Goldman, S., Yokota, H., Clark, A. J., and Kim, S.-H. (1988) Overexpression of archaeal proteins in *Escherichia coli*, *Biotechnol. Lett. 20*, 207−210.
30. LeMaster, D. M., and Richards, F. M. (1985) ^1H ^{15}N heteronuclear NMR studies of *Escherichia coli* thioredoxin in samples isotopically labeled by residue type, *Biochemistry 24*, 7263−7268.
31. Otwinowski, Z., and Minor, W. (1997) Processing of X-ray diffraction data collected in oscillation mode, in *Methods in Enzymology* (Carter, C. W. J., and Sweet, R. M., Eds.) pp 307−326, Academic Press, New York.
32. Leslie, A. G. W. (1992) Recent changes to the MOSFLM package for processing film and image plate data, in *Joint CCP4 + ESF-EAMCB Newsletter on Protein Crystallography 26*, 22−23.
33. Collaborative Computational Project, Number 4 (1994) The CCP4 suite: programs for protein crystallography, *Acta Crystallogr. D 50*, 760−763.
34. Terwilliger, T. C., and Berendzen, J. (1999) Automated MAD and MIR structure solution, *Acta Crystallogr. D 55*, 849−861.
35. McRee, D. E. (1999) XtalView/Xfit-a versatile program for manipulating atomic coordinates and electron density, *J. Struct. Biol. 125*, 156−165.
36. Brünger, A. T., Adams, P. D., Clore, G. M., Delano, W. L., Gros, P., Grosse-Kunstleve, R. W., Jiang, J.-S., Kuszewski, J., Nilges, N., Pannu, N. S., Read, R. J., Rice, L. M., Simonson, T., and Warren, G. L. (1998) Crystallography and NMR stystem (CNS): A new software system for macromolecular structure determination, *Acta Crystallogr. D 54*, 905−921.
37. Laskowski, R. A., MacArthur, M. W., Moss, D. S., and Thornton, J. M. (1993) PROCHECK: a program to check the stereochemical quality of protein structures, *J. Appl. Crystallogr. 26*, 283−291.
38. Toyoshima, C., Nomura, H., and Tsuda, T. (2004) Lumenal gating mechanism revealed in calcium pump crystal structures with phosphate analogues, *Nature 432*, 361−368.
39. Toyoshima, C., and Mizutani, T. (2004) Crystal structure of the calcium pump with a bound ATP analogue, *Nature 430*, 529−535.
40. Andersen, J. P., Vilsen, B., Collins, J. H., and Jørgensen, P. L. (1986) Localization of E1-E2 conformational transitions of sarcoplasmic reticulum Ca-ATPase by tryptic cleavage and hydrophobic labeling, *J. Membr. Biol. 93*, 85−92.
41. Clausen, J. D., Vilsen, B., McIntosh, D. B., Einholm, A. P., and Andersen, J. P. (2004) Glutamate-183 in the conserved TGES motif of domain A of sarcoplasmic reticulum Ca^{2+}-ATPase assists in catalysis of E2/E2P partial reactions, *Proc. Natl. Acad. Sci. U.S.A. 101*, 2776−2781.
42. Daly, S. E., Blostein, R., and Lane, L. K. (1997) Functional consequences of a posttransfection mutation in the H2-H3 cytoplasmic loop of the α subunit of Na,K-ATPase, *J. Biol. Chem. 272*, 6341−6347.
43. Seto-Young, D., Bandell, M., Hall, M., and Perlin, D. S. (1998) Differential exposure of surface epitopes in the β-strand region of LOOP1 of the yeast H^+-ATPase during catalysis, *J. Biol. Chem. 273*, 18282−18287.
44. Baekgaard, L., Fuglsang, A. T., and Palmgren, M. G. (2005) Regulation of plant plasma membrane H^+- and Ca^{2+}-ATPases by terminal domains, *J. Bioenerg. Biomembr. 37*, 369−374.
45. Cornelius, F., and Mahmmoud, Y. A. (2003) Direct activation of gastric H,K-ATPase by N-terminal protein kinase C phosphorylation. Comparison of the acute regulation mechanisms of H,K-ATPase and Na,K-ATPase, *Biophys. J. 84*, 1690−1700.
46. Rimessi, A., Coletto, L., Pinton, P., Rizzuto, R., Brini, M., and Carafoli, E. (2005) Inhibitory interaction of the 14-3-3ϵ protein

with isoform 4 of the plasma membrane Ca^{2+}-ATPase pump, *J. Biol. Chem. 280*, 37195−37203.

47. Walker, J. M., Tsivkovskii, R., and Lutsenko, S. (2002) Metallochaperone Atox1 transfers copper to the NH_2-terminal domain of the Wilson's disease protein and regulates its catalytic activity, *J. Biol. Chem. 277*, 27953−27959.
48. Tsivkovskii, R., MacArthur, B. C., and Lutsenko, S. (2001) The Lys1010-Lys1325 fragment of the Wilson's disease protein binds nucleotides and interacts with the N-terminal domain of this protein in a copper-dependent manner, *J. Biol. Chem. 276*, 2234−2242.
49. Sanders, C. R., and Myers, J. K. (2004) Disease-related misassembly of membrane proteins, *Annu. Rev. Biophys. Biomol. Struct. 33*, 25−51.
50. Hsi, G., and Cox, D. W. (2004) A comparison of the mutation spectra of Menkes disease and Wilson disease, *Hum. Genet. 114*, 165−172.

BI0610045